Acta Cryst. (1968). A24, 150

X-Ray Pendellösung Fringes in Darwin Reflection*

BY B. W. BATTERMAN AND G. HILDEBRANDT†

Department of Materials Science and Engineering, Cornell University, Ithaca, New York, U.S.A.

(*Received* 16 *August* 1967)

Oscillations have been observed in the tails of the Darwin curve from thin specimens of silicon. Dynamical theory predicts such oscillations (Pendellösung) for plane wave incident conditions in which two wave points on the same branch of the dispersion surface interfere and produce beating in the diffracted intensity. The usual Pendellösung is observed in transmission in which beating occurs between wave fields on different branches of the dispersion surface related by spherical rather than plane wave conditions. The present experiment uses an asymmetrically cut first crystal to increase the effective width of the incident wave and therefore approach the plane wave condition. Quantitative fringe measurements *versus* thickness are in fair agreement with theory. The intensity and contrast of the fringes are in poor agreement with theory. Several of the more important factors which reduce the contrast are discussed. With a relatively simple assumption, the observed and expected intensity dislocations can be brought into good agreement.

Introduction

Pendellösung, in the sense of dynamical diffraction, refers to the beating inside a crystal of two wave fields which are coherently related. This phenomenon has been observed in the transmission case first by Kato & Lang (1959) and utilized by many other investigators to give important confirmations of the predictions of the dynamical theory as well as to arrive at accurate determinations of the scattering factors of certain materials (Hattori, Kuriyama, Katagawa & Kato, 1965; Hart, 1966; Batterman & Patel, 1966). In all of these cases the beating is between two wave fields which are coherently related because of the spherical nature of the incident wave front. In all the transmission cases (the so-called Laue case) the two beating wave fields have their tiepoints on separate branches of the dispersion surface. In the reflection case, beating should occur between wave points on the same branch of the dispersion surface whose wave vectors are coherently related by plane wave not spherical wave criteria. Ewald (1933) first predicted Pendellösung in the reflection case. This is discussed in some detail in the next section.

We have observed this Pendellösung between such wave fields for the case of Darwin reflection from thin perfect crystals of silicon. To the best of our knowledge this is the first experimental verification of this type of Pendellösung phenomenon.

Theory

Diffracted intensity from thin slabs

The dispersion surface for the usual Pendellösung effect in transmission is given in Fig. 1. Wave points A and B would be selected by an infinite incident plane wave whose outside wave point is P. Beating would occur between wave vector K_{HA} and K_{HB} (as well as K_{0A} and K_{0B} which are not shown in the Figure). Two factors, however, prevent this from being the case. One is, that in the usual experimental arrangement the range of incident angles is much larger than the reflection width so that all tiepoints on both branches are excited and interference between all tiepoints can take place. The other factor is that the incident wave front is usually limited by a narrow slit, so that the waves of the different tiepoints which have different Poynting vectors diverge in the crystal medium and no longer can superpose and exhibit the Pendellösung effect. Thus, in Fig. 1, the Poynting vectors S_A and S_B, which are normal to the dispersion surface, can make a large angle with one another (up to a maximum of 2θ). The wave point A' is also coherently excited and the Poynt-

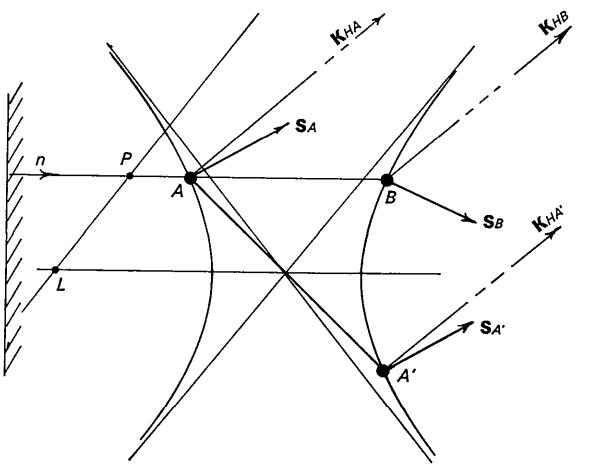

Fig. 1. Dispersion surface and tiepoints for symmetric Laue transmission. Tiepoints A and B are related by plane wave conditions while A and A' interfere through spherical wave criteria.

* Research supported by Advanced Projects Agency through the Materials Science Center at Cornell University.

† Present address: Fritz-Haber Institut, Berlin-Dahlem, Germany.

ing vector $\mathbf{S}_{A'}$ is parallel to $\mathbf{S}_A$ and it is these two wavepoints which interfere with the beat wave vector given by $\mathbf{K}_{HA}-\mathbf{K}_{HA'}=\mathbf{K}_{0A}-\mathbf{K}_{0A'}$ not $\mathbf{K}_{HA}-\mathbf{K}_{HB}$ which the plane wave theory would predict.

The important criteria of wave-front coherency which must be fulfilled in order to observe Pendellösung in the Bragg case are discussed in the next section. For the present we will discuss only the usual infinite plane wave treatment.

Von Laue (1941) and Zachariasen (1945) have calculated the reflection curves for non-absorbing thin crystals in reflection geometry. When the crystal is thin, instead of the usual Darwin top-hat curve with a range of total reflection, the thin crystal curve has tails of an oscillating nature having zeros at regular intervals which depend on the crystal thickness (see Fig. 3). When absorption is present the curves are modified somewhat and nodes of zero intensity are no longer present. James (1963) has worked out in detail the case including absorption. Rather than repeat James's derivation here we will just give the results and present instead a physical explanation of the origin of the Pendellösung phenomenon for reflection from a thin slab.

In Fig. 2(*a*) we show the dispersion surface for the symmetric reflection case where the two wave points (1) and (2) are selected by the incident conditions. Fig. 2(*b*) shows the actual experimental geometry in the same orientation as in Fig. 2(*a*) with the amplitudes of the inside and outside waves shown schematically. We assume for the moment *no absorption*. We will use notation consistent with that in the review paper of Batterman & Cole (1964). The boundary conditions on amplitudes (Batterman & Cole, 1964, sec. 2.4) demand that at the upper surface, $Z=0$;

$$E_0^i=E_{01}+E_{02} \tag{1}$$

$$E_H^i=E_{H1}+E_{H2} \tag{2}$$

and at the lower surface, $Z=d$.

$$0=E_{H1}\exp(-2\pi i\mathbf{K}_{H1}\,.\,\mathbf{r}')+E_{H2}\exp(-2\pi i\mathbf{K}_{H2}\,.\,\mathbf{r}') \tag{3}$$

where r' lies in $Z=d$. The electric field associated with any wave is of the form $\varepsilon_i=E_i\exp(-2\pi i\mathbf{K}_i\,.\,\mathbf{r})$. Equation (3) states that no diffracted ray passes through the lower surface. E_0^i and E_H^i are the amplitudes of the outside incident and diffracted waves respectively and E_0^e is the transmitted amplitude through the bottom of the slab. Equation (3) can be written

$$E_{H1}/E_{H2}=-e^{-i\varphi} \tag{4}$$

where $\varphi=2\pi i(\mathbf{K}_{H2}-\mathbf{K}_{H1}\,.\,r')=2\pi i|\mathbf{K}_{H2}-\mathbf{K}_{H1}|d$ for the symmetric case where $\mathbf{K}_{H2}-\mathbf{K}_{H1}$ is normal to the slab. Equation (4) states that at any point in the crystal the two waves travelling in the diffracted beam direction have the same absolute amplitude. These two waves have their wave vectors very nearly parallel but different in magnitude by $|\mathbf{K}_{H2}-\mathbf{K}_{H1}|$, which is the chord connecting the two wave points on a given branch of the dispersion surface. These two infinite plane waves therefore beat with a period equal to $|\mathbf{K}_{H2}-\mathbf{K}_{H1}|^{-1}$ with nodes of intensity in planes parallel to the surface of the crystal slab. The diffracted intensity which by equation (2) is the sum of these two waves at the entrance surface will be zero whenever this nodal plane is coincident with the surface. As the angle of incidence is changed the beat period changes and nodal planes are swept through the surface cancelling the diffracted wave.

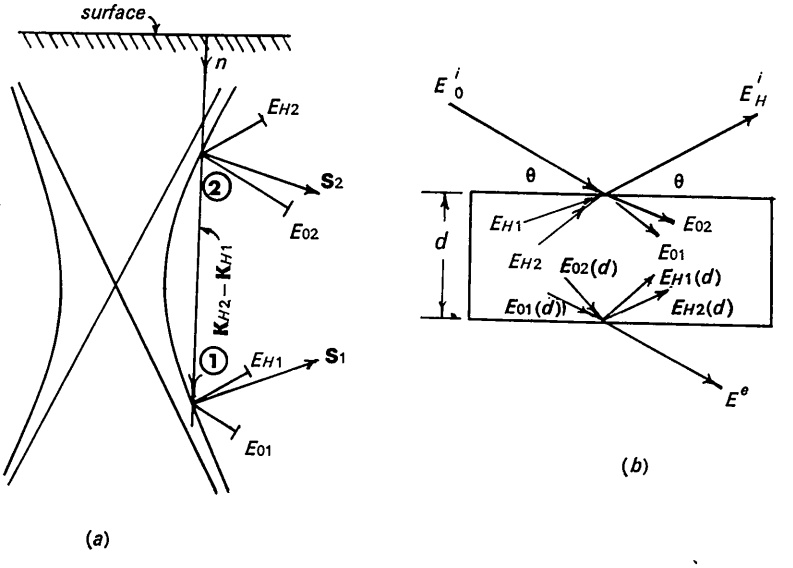

Fig. 2. (*a*) Dispersion surface for symmetric Bragg reflection. E_{Hi} and E_0i schematically represent the amplitudes at each of the two wave points ($i=1,2$). (*b*) Wave amplitudes that must satisfy the boundary conditions at the two surfaces leading to equations (1), (2) and (3). The ordinate for the tails is reduced by a factor of 5.

Wave field (1) composed of $\mathbf{K}_{01}$ and $\mathbf{K}_{H1}$ has a Poynting vector $\mathbf{S}_1$ towards the crystal surface. It is tempting to say that this field is generated by reflection from the lower surface (it is indeed just this wave field that *does not exist* for the infinite crystal), although this is not strictly correct. It must be remembered that we are dealing with infinite plane waves, and the concept of wavefield (2) arriving at the bottom surface and generating (1) loses its significance.

When absorption is taken into account, wave field (1) which arrives at the upper surface from within the crystal has suffered attenuation, whereas field (2) which is just entering the crystal has not yet suffered absorption. Thus, the two waves E_{H1} and E_{H2} no longer have the same absolute amplitude at the surface and nodes of zero diffracted intensity disappear. However, since we usually are dealing with quite thin crystals the absorption effects should be quite small and oscillations nearly go to zero. It is worthwhile pointing out that since in the Bragg geometry we always deal with two wave fields on the same branch, the absorption of each field is the same (in the symmetric case) but since one field [(1) in Fig. 2(*a*)] propagates towards the surface, its dynamical absorption coefficient is the negative that of wave field (2), because the intensity in the field increases as one goes deeper in the crystal. The equations which describe the reflection coefficient $R(\eta')$ are given below for the case of *symmetric reflection* from a slab of thickness d. The equations are basically those of James (1963) with a slight change in notation to be consistent with that of Batterman & Cole (1964).

The data will be presented on an η' scale which is related to the deviation from the uncorrected Bragg angle, $\Delta\theta$, by

$$\eta' = (-\Delta\theta \sin 2\theta + \Gamma F_0')/|P|\Gamma F_H' \qquad (5)$$

where $\Gamma = (e^2/mc^2)\lambda^2 N/\pi$, $F_H = F_H' + iF_H''$ is the structure factor for the hkl reflection, $P = 1$ or $\cos 2\theta$ for the σ and π states of polarization, N is the number of unit cells per unit volume, λ the wave length and (e^2/mc^2) the classical electron radius. The reflection curve is divided into three ranges: range (1), $\eta' < -1$; range (2), $-1 < \eta' < +1$; range (3), $n' > 1$. A complex quantity v is defined by: range (1), $\eta = -\cosh v$; range (2), $\eta = \cos v$; range (3), $\eta = \cosh v$, where $\eta = \eta' + i\eta''$ and $v = v' + iv''$. For range (1) the reflection coefficient* is given by

$$R_1(\eta') = \frac{\cosh\varphi - \cos\beta d}{\cosh(\varphi + 2v') - \cos(\beta d - 2v'')} \qquad (6)$$

$$\varphi = -\mu_z(\eta')d = -(\mu_0 \sin\theta)(\eta' - |P|\varepsilon)/(\eta'^2 - 1)^{\frac{1}{2}} \qquad (7)$$

$$\beta = -(2\pi/\Delta_0)(\eta'^2 - 1)^{\frac{1}{2}} \qquad (8)$$

$$\eta'' = \frac{F_0''}{|P|F_H'}(1 - |P|\eta'\varepsilon) \qquad (9)$$

$$v'' = -\eta''/(\eta'^2 - 1)^{\frac{1}{2}}, \qquad (10)$$

where $\mu_z(\eta')$ is the dynamical absorption coefficient, μ_0 the normal linear absorption coefficient, $\varepsilon = F_H''/F_0''$ and

$$\Delta_0 = \frac{\pi \sin\theta}{(e^2/mc^2)\lambda F_H' N} \qquad (11)$$

is called the beat period. In all cases we have taken F_H''/F_H' to be a small quantity and to second order $|F_H| = F_H'$. The quantity $(\eta'^2 - 1)^{\frac{1}{2}}/\Delta_0$ gives the length of the chord between the two wave points in Fig. 2(*a*).

For range (2)

$$R_2(\eta') = \frac{\cosh\varphi - \cos\beta d}{\cosh(\varphi + 2v'') - \cos(\beta d + 2v')}, \qquad (12)$$

where

$$\beta = -(\mu_0/\sin\theta)(\eta' - |P|\varepsilon)/(1 - \eta'^2)^{\frac{1}{2}} \qquad (13)$$

$$\varphi = -(2\pi d/\Delta_0)(1 - \eta'^2)^{\frac{1}{2}} \qquad (14)$$

$$v' = -\eta''/(1 - \eta'^2)^{\frac{1}{2}}.$$

For range (3), $R_3(\eta')$ is obtained from $R_1(\eta')$ by changing the sign before the v' and v'' terms in equation (6)

* The equations for the reflection coefficients correspond to equations 65·8 and 65·12 of James (1963).

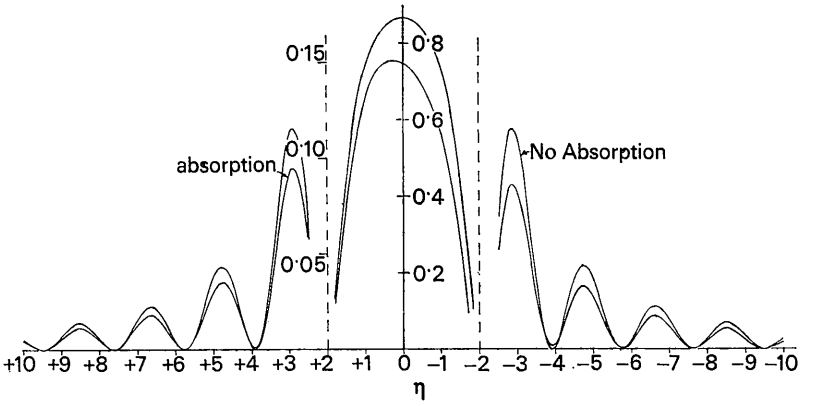

Fig. 3. Theoretical diffraction curve from a thin slab with $d/\Delta_0 = 0{\cdot}53$ [Equation (11)]. The upper curve is for no absorption [Equations (15) and (16)], while the lower curve includes the affect of absorption [Equations (6) and (12)]. The curve is plotted with η' increasing to the left so that Bragg angle increases to the right. The ordinate for the tails is reduced by a factor of 5.

and v'' is given by equation (10) with the minus sign before η'' changed to plus. F_0'' is related to the linear absorption coefficient μ_0 by $F_0''=\mu_0/2\pi k\Gamma$. The above equations are approximations valid when the absorption terms are small and η' is not very close to unity.

When absorption is neglected, $v''=\mu_0=0$ and the above equations simplify to

$$R_1=R_3=\frac{1-\cos\beta d}{\cosh 2v-\cos\beta d}, \tag{15}$$

where β is given by equation (8) and

$$R_2=\frac{\cosh\varphi-1}{\cosh\varphi-(2\eta^2-1)}, \tag{16}$$

where φ is given by equation (14).

For the non-absorbing case we see from equations (15) and (8) that zeros in the reflected intensity correspond to values of η' such that

$$\frac{d}{\Delta_0}(\eta'^2-1)^{\frac{1}{2}}=m, \tag{17}$$

where m is an integer. For large m, adjacent zeros of diffracted intensity are separated by $\delta\eta=\Delta_0/d$. It can be seen from equation (6) that with absorption the numerator will always be greater than zero since $\cosh x>1$, and zeros in the diffracted intensity will not occur. We plot in Fig. 3 the theoretical curves for crystal with $d/\Delta_0=0{\cdot}53$, which corresponds to the 333 reflection of silicon and a crystal thickness of 13·6 microns. As expected, the affect of absorption is to eliminate zero nodes and is asymmetric. The absorption has a larger effect on the high angle side (negative η) corresponding to wave points on the branch of the dispersion surface indicated in Fig. 2(*a*).

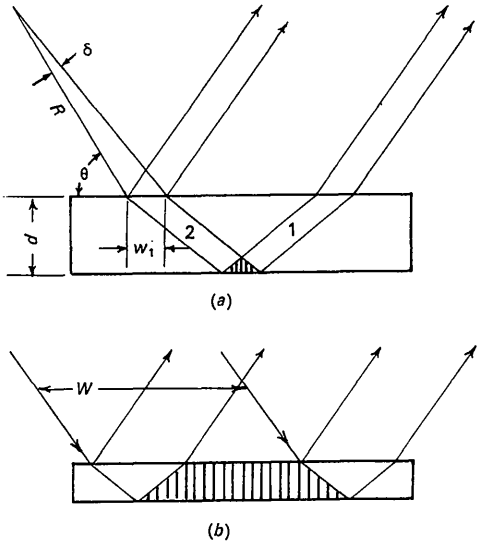

Fig. 4. (*a*) Diffraction from a thin slab when the coherence width w_1 is small compared with the thickness. The shaded area is the region of overlap of the two wave fields. (*b*) As in (*a*), but with a width W which is large compared with the thickness. In this case the wave fields overlap at the upper surface.

Problem of coherency of the wave front

Aside from the expected experimental considerations of crystalline perfection of the specimen, freedom from bending and parallelness of the faces of the slab, one must consider the lateral coherence of the X-ray wave field used in the experiment.

The importance of this property (and our use of the term coherency) can be illustrated in the following way: Consider a monochromatic point source of X-rays at a distance R from the crystal slab [Fig. 4(*a*)]. Since the crystal we are investigating has both a reflection width and a fringe separation of a few seconds of arc, we need as the probing incident beam an angular width of say 0·5 sec or less. The width w_1, at the crystal corresponding to this angular range, we will call the lateral coherence, and from Fig. 4(*a*)

$$w_1=R\delta/\sin\theta\,. \tag{18}$$

In our experiment $R=25$ cm and $\theta=47{\cdot}5°$ so that $w_1\simeq 1$ micron. This represents the width of the coherent wave front and it is roughly within this range we can consider the interaction of internal wave fields to supply the Pendellösung phenomenon we are looking for. More explicitly, it is only over the lateral extent w_1 that wave field (2) in Fig. 2(*a*) is excited. This field must propagate into the slab, reflect at the back face and generate field (1) which propagates towards the surface. Thus, in Fig. 4(*a*), only in the shaded region will the two wave fields overlap and Pendellösung occur. Clearly the situation shown in Fig. 4(*a*) will not produce any beats, because nowhere at the upper crystal surface do the two fields overlap. In other words, we are nowhere near satisfying the criteria necessary for the infinite plane wave treatment. What we would like to have is something more like the situation in Fig. 4(*b*) where a large overlapping region exists at the upper surface.

In the present experiment we are dealing with the 333 reflection of silicon. This reflection was picked as a compromise between two experimental parameters: slab thickness *vs* fringe separation. For 333 the Darwin width is 1·9″ which is more difficult to work with than 111, which has a width of 7″. However, the crystal thickness necessary to get reasonable fringe separation is about 3 microns for 111 while for 333 it is the order of 15 microns. 5-Micron crystals are very difficult to mount without bending so the compromise was made with the 333 reflection, even though the fringe separation will tend to be smaller than for 111.

Therefore, with a crystal thickness of about 15μ and a coherence width of 1μ, we would have the undesirable situation in Fig. 4(*a*), and consequently, see no Pendellösung effect. Fortunately, there is available a relatively simple means of extending the lateral coherence of the wave front and still isolate a beam of very narrow angular width.

Here we take advantage of the properties of an asymmetrically cut first crystal to narrow the angular

range of the Darwin curve (Renninger, 1961; Kohra, 1962). Fig. 5 shows an asymmetrically cut first crystal where the primary beam makes an angle of α with the crystal surface. According to dynamical theory the angular width of the diffracted rays, δ_2, will be

$$\delta_2=\delta_0\left(\frac{\sin\alpha}{\sin(2\theta-\alpha)}\right)^{\pm} \tag{19}$$

where δ_0 is the angular width of total reflection for the symmetric Bragg case (the usual Darwin width). In our case $\theta=47{\cdot}5°$ and $\alpha=2°$, so that δ_2 is 0·19 that of the Darwin width. While equation (19) refers to the width of reflected beam, a similar expression gives δ_1, the angular range of incident beam that will produce a reflected beam of angular range δ_2:

$$\delta_1=\delta_0\left(\frac{\sin(2\theta-\alpha)}{\sin\alpha}\right)^{\pm} \tag{20}$$

It is clear from equations (19) and (20) that $\delta_2/\delta_1=\sin\alpha/\sin(2\theta-\alpha)$ and for our case this is a factor of 0·0348. That is, the asymmetric cut crystal acts like an X-ray condensing lens reducing the divergence of a beam by a factor of nearly 30. From the geometry of Fig. 5 it can be easily shown that

$$W=R\delta_1\sin(2\theta-\alpha)/\sin\alpha\sin\theta\,, \tag{21}$$

where W is the lateral extent of the beam parallel to the diffracting planes with angular divergence δ_2. Fig. 5 represents our experimental set up in which both the asymmetrical first crystal and the thin slab are set for 333 diffraction. The 333 Darwin width δ_0 is 1·9″ for silicon with Cu $K\alpha$ radiation. The incident beam on the specimen has an angular width $\delta_2=0{\cdot}37''$ [equation (19)] and has a lateral width (all rays within this width are parallel to 0·37″) of $W=508$ microns. With a point source at distance R and the same angular width δ_2 seen by the specimen, we would get the much smaller width $W_1=R\delta_2/\sin\theta$ [equation (18)]. Dividing this into (21) and combining with equations (19) and (20) we get

$$\frac{W}{W_1}=\left(\frac{\sin 2\theta-\alpha}{\sin\alpha}\right)^2 \tag{22}$$

The magnification in lateral width according to this would be $(28{\cdot}8)^2=830$. The net result of the asymmetrically cut first crystal is to provide a beam that would be more nearly that of Fig. 4(*b*) rather than 4(*a*) and we consequently would expect to see the Pendellösung phenomenon. Thus, it is possible to use the asymmetric cut crystal as a means of providing an X-ray wave front of large lateral width with a small angular divergence. In other words, the wave front can be made to approach closer to that of an infinite plane wave than would be possible by more conventional arrangements.

Experimental

The experimental arrangement is shown schematically in Fig. 5. Cu $K\alpha$ radiation from the point focus (1×1 mm^2) was incident on the asymmetrically cut first silicon crystal, C_1 and the second crystal C_2 adjusted for diffraction in the $(3,\bar{3})$ parallel double crystal spectrometer arrangement. Since the Bragg angle is 47·5°, which is quite close to 45°, the reflected Cu $K\alpha$ radiation from C_1 was almost completely perpendicularly polarized. As stated in the previous section, the first crystal is cut with an asymmetry angle α of 2°. The second crystals were thin silicon lamellae with (111) faces with an area of about 1 cm^2 and thickness between 7 and 30 μm. They were of the type used for $p-n$ junction particle detectors and were prepared by T. C. Madden of the Bell Telephone Laboratories (see Madden & Gibson, 1964). The slit S_1 had a pinhole with a diameter of $\simeq2$ mm allowing the first crystal to produce reflected radiation along its entire width. S_2 was a pinhole of 0·5 mm diameter which could be

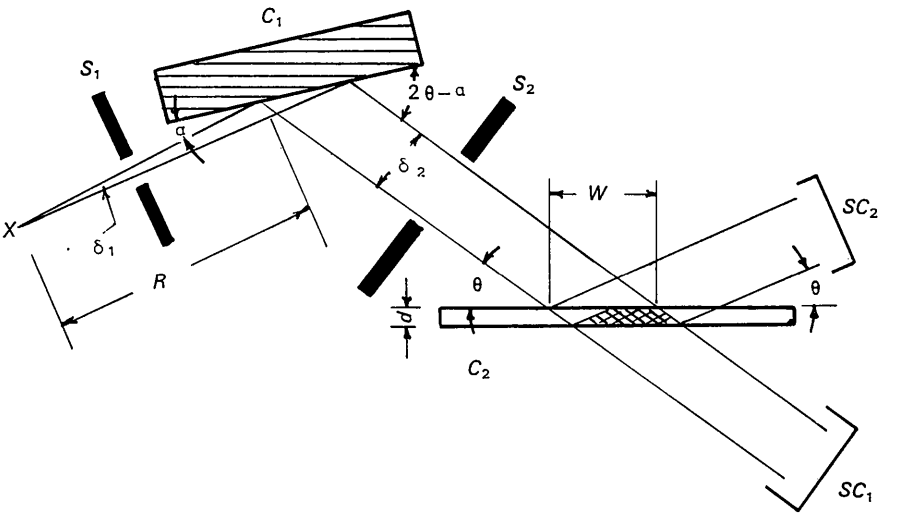

Fig. 5. Experimental arrangement with beam divergences. X, Cu target anode, S_1, S_2 pinholes; $C1$, 1st crystal Si(333) and $C2$, thin silicon of thickness d; SC_1, SC_2 are two NaI scintillation counters.

translated horizontally so that different portions of the thin crystals could be examined. The scintillation counter SC_1 was used to adjust the first crystal and to measure the thickness of C_2 by absorption precisely at that point on its face which produced the symmetrically diffracted beam measured with counter SC_2.

The angular position of the specimen could be adjusted to a small fraction of a second of arc either in small steps by hand, or continously with a synchronous motor. The thin second crystal was extremely sensitive to thermal and mechanical disturbances as well as minute air currents. To minimize these effects, the entire spectrometer was enclosed within a copper shell covered with insulating material. Both the shell and the spectrometer were in good thermal contact with copper tubing in which thermostatically controlled water was circulated.

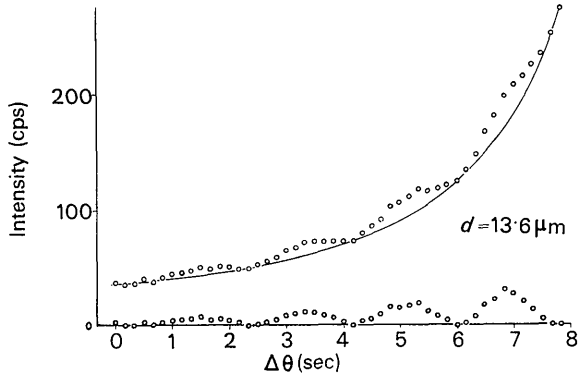

Fig. 6. Experimental results for a 13·6 μm crystal in the angular range from 12 to 4″ on the low angle side of the main maximum. The count rate at the peak is 3400 cps. The lower curve is obtained by subtracting the monotonic curve from the data.

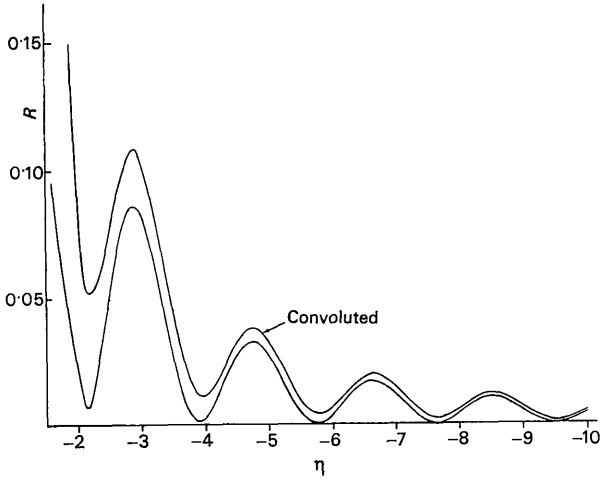

Fig. 7. The effect of convolution on the theoretical diffraction curve. The lower curve is taken from Fig. 3 (with absorption). The upper curve is essentially the convolution of the lower curve with the asymmetric Darwin–Prins curve of the first crystal.

The most critical problem was the mounting of the second crystal to its holder. This was done with a small amount of beeswax near the corner of the crystal. The following properties were found if the contact between specimen and its holder was too light. The angular position of C_2 was not stable enough, it changed even after several days. The crystal was so sensitive to vibrations that it was impossible to get a record of the reflection curve with the synchronous motor which was directly attached to the goniometer. Even microphonic effects could sometimes be observed (*i.e.* sensitivity to certain acoustic frequencies). If on the other hand, the contact was too firm, deformation was introduced into the crystal leading to a broadening of the reflection curves and a diminishing or complete loss of fringe contrast. The proper amount of contact was determined strictly by trial and error.

To check the alignment of the spectrometer, we used a 2 mm thick silicon crystal in position C_2. The theoretical half width (full width at half maximum) for a non-absorbing crystal is $3\sqrt{2}|P|\Gamma F_H/2\sin\theta$ [this is the range $\Delta\eta'=3\sqrt{2}/2$ in equation (5)]. The range of total reflection is $2|P|\Gamma F_H/\sin\theta$ corresponding to $\Delta\eta'=2$ in equation (5). The half-width using the Hattori *et al.* (1965) experimental value of $F_H(333)=5{\cdot}9$, which includes thermal motion, is 1·94″ for the symmetrically cut crystal and 0·39″ for the asymmetrically cut first crystal. The convoluted width should therefore be somewhat less than 2·3″. The measured value of 2·55″ was 10% higher, which is in reasonable agreement with theory.

The thin crystal was investigated over its face by moving pinhole S_2 in a plane normal to Fig. 5. The results of many attempts with several silicon wafers may be summarized as follows: A half-width in the range 2·7 to 3·5 seconds of arc was the necessary but not sufficient condition to detect fringes which could be quantitatively evaluated. Our best results were obtained in a particular area of 4×8 mm^2 over which the thickness ranged from 7 to 23 microns.

For each measurement the curve was point-counted in steps of 0·16″ starting from a position 12″ from the peak maximum. The fringes, when detected, covered a range of about 9″ and the curves comprised some 50 measurements each of 1 to 2 minute duration. The stability of the arrangement was not good enough to guarantee that the crystal position would remain constant over the total measurement time. Therefore, after about 10 measurements the zero position was checked by determining the position of a given intensity point on the steep portion of the main maximum. The fringe heights tended to be different on the high and low angle sides consistent with that shown in Fig. 3. The low angle side, involving the field with lowest absorption, always gave the best fringe contrast and for some runs this was the only side measured.

For each fringe measurement the crystal thickness was determined by the absorption in the foil measured with counter SC_1. For this determination the value of

$\mu_{Si,\,Cu\,K} = 144$ cm^{-1} was used. This was previously measured by one of the authors (Hildebrandt, 1968) and is in good agreement with values of Lefeld–Sosnowska (1964) 150 cm^{-1} and Cooper (1965) (interpolated) 148 cm^{-1}.

To prove that the fringes were not the result of any mechanical periodicity, a run was made with the specimen replaced by a thick silicon crystal. The data were taken with the identical statistical counting as with the thin lamella. A smooth monotonic peak with no hint of any fringes was observed. We also measured the entire angular range of one thin crystal region point by point with random selection of the angular setting for the point counting. For each point the $\Delta\theta$ deviation was measured from a fixed intensity point on the flank of the central maximum. The curve so obtained was the same as that taken with equal incremental steps in $\Delta\theta$.

Results

The best fringe contrast was obtained with one silicon lamella. Seven areas were investigated with a thickness range between 7 and 23 μm. One of the measurements with good fringe contrast for a region of thickness 13·6 μm is shown in Fig. 6. We include also the oscillatory portion which is obtained by subtracting a smoothed curve from the data. A comparison with Fig. 3 shows that the theoretical curve, even with absorption, has very much better resolved oscillations. One expected source of broadening is the finite diffraction width of the first crystal. The extent of this broadening was determined by convoluting the Darwin–Prins curve of the asymmetrically cut first crystal with the curve of Fig. 3 [Equations (15) and (16) without absorption]. Since the affect of absorption is small, the calculation was considerably simplified by using equations (15) and (16) rather than the more exact equations (6) and (12). The affect of the first crystal broadening is shown in Fig. 7. The fringe contrast is reduced sharply. For the first fringe the low point is raised considerably above zero and for all peaks the valley between the fringes is filled to a fairly large extent. This gives closer agreement to experiment, but still is a long way from reproducing the observations.

At this point we can only enumerate some of the other possible broadening mechanisms and speculate to what extent they are involved. Our calculated lateral coherence width of 508 microns is only for those points on the source which have coherent widths centered in the slit system. For certain regions of the source, the full coherent lateral width will not be seen by the specimen and the effective coherent width will be much smaller than this value. A width of 500 micron will give a loss of overlap region ($\geqslant$ minus shaded area at upper surface in Fig. 5) of 5% for a 13 micron crystal and this loss will increase as the effective W decreases. That fraction outside of the overlap regions will produce no fringes and add a monotonic background to the fringe curves.

For the convolution in Fig. 7 it was tacitly assumed that each point within the width of W on the specimen was illuminated with rays having the full range δ_2 from the first crystal. This is actually not the case since for each point on the source the angle of the diffracted ray from the first crystal will vary continuously along W over the range of δ_2. This results in reducing the effective coherence width and also the overlap region and will therefore contribute to the broadening and reduction of fringe contrast.

Slight distortions of the crystal will affect the energy flow **S** very drastically. One of the authors (Hildebrandt, 1959) has shown that the wave field which, in a perfect lattice, would normally have energy flow into the crystal, can actually change its direction owing to a slight bending of the planes and come out through the entrance surface. Bonse (1964) studied this effect in the vicinity of a dislocation. Any such distortion would, of course, adversely affect the fringe contrast.

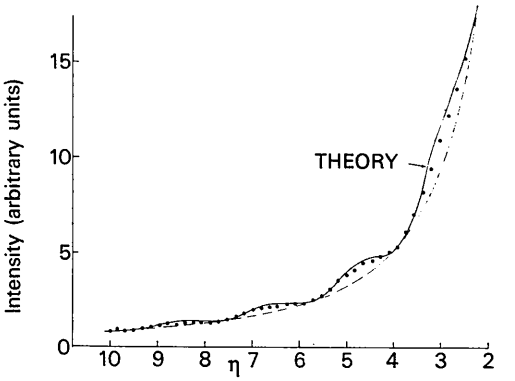

Fig. 8. The data points are the same as those in Fig. 6. The dashed curve is the tail of a Darwin curve from a thick crystal. The solid curve is the sum of the Darwin curve and the Pendellösung curve in Fig. 7 normalized in the ratio of 10:1.

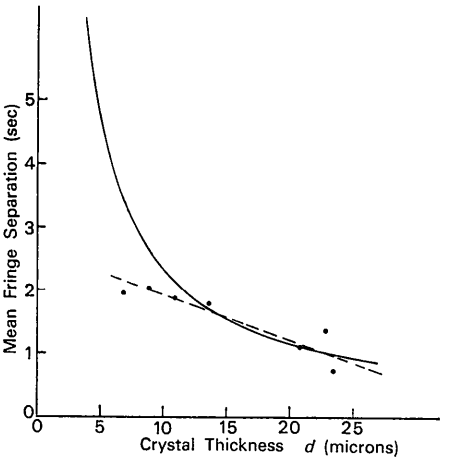

Fig. 9. Observed mean fringe separation *versus* thickness. The solid curve is the mean fringe separation predicted for a beat period $\Delta_0 = 25{\cdot}6$ μm [Equations (11) and (23)].

Most of these effects would tend to destroy the necessary plane wave conditions and reduce the fringe visibility, and in certain cases actually alter the fringe separation. One approximation that can be made is to assume that all the effects that would destroy the Pendellösung would merely add to a monotonic background similar to that of the Darwin curve from a thick crystal. By trial and error we have combined the convoluted curve of Fig. 7 with a monotonic Darwin curve to get the best agreement with our observations. Fig. 8 gives the curve for a ratio of Darwin to Pendellösung of about 10:1. The solid curve represents the sum of the two functions and the monotonic dashed curve is the tail of a Darwin thick crystal curve. The points are the experimental values. The agreement between observation and the solid curve is quite good.

In addition to the shape of the fringes we also measured the mean fringe separation. To the precision with which this value can be determined, we can safely neglect unity compared to η'^2 in equation (17) and have the simple relation between fringe separation f and thickness d

$$f=\Delta_0/d\,. \qquad (23)$$

In Fig. 9 we give the experimentally observed separations *vs* thickness as well as the relationship predicted by equation (23) with a value of $\Delta_0=25{\cdot}6$ μm calculated from the measured $F(333)$ of 5·9.

The scatter is quite large but the data points lie more or less on a straight line tangential to the theory curve at about 18 μm. The deviation for small thickness could possibly be attributed to bending for which the thinner regions would be most sensitive. The agreement with theory is not too satisfactory, but is probably within the rather large uncertainty of the measurements.

Conclusions

Our experiment has verified the existence of the Pendellösung phenomena in the case of Bragg reflection from the surface of a thin crystal. This type of Pendellösung involves the interference of wave fields on the same branch of the dispersion surface and as such is more within the framework of a plane wave, rather than a spherical wave phenomenon.

We have pointed out that an asymmetrical reflection from a perfect crystal has the effect of increasing the lateral coherence of an X-ray beam. By this we mean that asymmetric reflection can produce a beam whose lateral width for a given angular divergence is several orders of magnitude larger than could be obtained by isolating a bundle of that same divergence from a point source of X-rays. The observation of the Pendellösung fringes is an implicit verification that such enhancement of lateral width does indeed take place.

We wish to thank T. C. Madden of the Bell Telephone Laboratories for providing the silicon wafers and Dr P. Ho of Cornell who programmed the computer calculations.

References

BATTERMAN, B. W. & COLE, H. (1964). *Rev. Modern Phys.* **36**, 681.
BATTERMAN, B. W. & PATEL, J. R. (1966). *Acta Cryst.* **21**, A14. *J. Appl. Phys.* To be published.
BONSE, U. (1964). *Z. Physik*, **177**, 543.
COOPER, M. J. (1965). *Acta Cryst.* **18**, 813.
EWALD, P. P. (1933). *Handb. Physik*, **23**, 291.
HART, M. (1966). *Z. Physik*, **89**, 269.
HATTORI, H., KURIYAMA, H., KATAGAWA, T. & KATO, N. (1965). *J. Phys. Soc. Japan*, **20**, 988.
HILDEBRANDT, G. (1959). *Z. Kristallogr.* **112**, 340.
HILDEBRANDT, G. (1968). To be published.
JAMES, R. W. (1963). *Solid State Physics*, **15**, 132.
KATO, N. & LANG, A. R. (1959). *Acta Cryst.* **12**, 787.
KOHRA, K. (1962). *J. Phys. Soc. Japan*, **17**, 589.
VON LAUE, M. (1941). *Röntgenstrahlinterferenzen*, Leipzig: Akademische Verlagsges.
LEFELD-SOSNOWSKA, M. (1964). *Phys. Stat. Sol.* **7**, 449.
MADDEN, T. C. & GIBSON, W. M. (1964). *IEEE Transact. Nuclear Science* NS11, no. 3, 254.
RENNINGER, M. (1961). *Z. Naturforsch.* **16A**, 1110.
ZACHARIASEN, W. H. (1945). *Theory of X-Ray Diffraction in Crystals*. New York: John Wiley.

Acta Cryst. (1968). A**24**, 157

Reciprocity Theorem in Optics and its Application to X-ray Diffraction Topographs

BY N. KATO
Department of Applied Physics, Faculty of Engineering, Nagoya University, Nagoya, Japan

(*Received* 10 *June* 1967)

The reciprocity theorem is applied to X-ray diffraction topographs. The intensity distribution of a traverse-type topograph is obtained by knowing the integrated intensity of the section-type topograph which would be produced with the same crystal by X-rays emitted from a source located virtually at the point concerned. This relation holds in general irrespective of the shape, absorption and distortion of the crystal and the polarization of X-rays.

Introduction

This paper describes a relation between two kinds of X-ray diffraction topograph of transmission type; namely section and traverse topographs. They are most fundamental in transmission diffraction topography. The experimental procedures of taking these topographs are described by Lang (1958, 1959) and Kato & Lang